

Article

Optimal Dispatching of Smart Hybrid Energy Systems for Addressing a Low-Carbon Community

Wei Wu *, Shih-Chieh Chou and Karthickeyan Viswanathan

Department of Chemical Engineering, National Cheng Kung University, Tainan 70101, Taiwan

* Correspondence: weiwu@gs.ncku.edu.tw

Abstract: A smart hybrid energy system (SHES) is presented using a combination of battery, PV systems, and gas/diesel engines. The economic/environmental dispatch optimization algorithm (EEDOA) is employed to minimize the total operating cost or total CO₂ emission. In the face of the uncertainty of renewable power generation, the constraints for loss-of-load probability (LOLP) and the operating reserve for the rechargeable battery are taken into account for compensating the imbalance between load demand and power supplies. The grid-connected and islanded modes of SHES are demonstrated to address a low-carbon community. For forecasting load demand, PV power, and locational-based marginal pricing (LBMP), the proper forecast model, such as long short-term memory (LSTM) or extreme gradient boosting (XGBoost), is implemented to improve the EEDOA. A few comparisons show that (i) the grid-connected mode of SHES is superior to the islanded-connected mode of SHES due to lower total operating cost and less total CO₂-eq emissions, and (ii) the forecast-assisted EEDOA could effectively reduce total operating cost and total CO₂-eq emissions of both modes of SHES as compared to no forecast-assisted EEDOA.

Keywords: power dispatch; forecasting; optimization; operating reserve; smart hybrid energy system



Citation: Wu, W.; Chou, S.-C.; Viswanathan, K. Optimal Dispatching of Smart Hybrid Energy Systems for Addressing a Low-Carbon Community. *Energies* **2023**, *16*, 3698. <https://doi.org/10.3390/en16093698>

Academic Editor: Branislav Hredzak

Received: 3 March 2023

Revised: 13 April 2023

Accepted: 21 April 2023

Published: 25 April 2023



Copyright: © 2023 by the authors. Licensee MDPI, Basel, Switzerland. This article is an open access article distributed under the terms and conditions of the Creative Commons Attribution (CC BY) license (<https://creativecommons.org/licenses/by/4.0/>).

1. Introduction

Nowadays, the worldwide power system would rapidly develop towards a low-carbon smart community energy system where intermittent renewable energy sources such as solar PV and wind energy should rely on energy storage systems to keep an uninterrupted energy supply [1,2]. In coping with peak loads of the community energy system with non-renewable and renewable energy resources, the hybrid energy management system has become a crucial mechanism to ensure distributed energy resources in intelligent, secure, reliable, and coordinated ways [3–5]. The hybrid energy management system was responsible for power dispatching, energy savings, and allocating power among generators, so a prediction-based optimization strategy could play a role in balancing the use of diesel generators and emergency batteries [6]. Regarding the optimal dispatching of intermittent renewable energy sources, a probabilistic approach was used to solve the economic dispatch problem considering the uncertainty of wind power generation and generators' reliability [7]; however, the uncertainty and variability problem of these sources has brought many complications to handling the complex hybrid energy systems. From economic, energy, and environmental perspectives, the integration of renewable energy sources in the electrical grid was a promising way to reduce the total operating cost according to different operational scenarios [8], but the optimal dispatching of intermittent renewable energy and non-renewable sources was not addressed.

For addressing a smart hybrid energy system, a machine learning-based optimized energy dispatch scheme was implemented to maintain the voltage stability in a power plant operated in an islanded mode [9], a smart hybrid energy system used the genetic algorithm and artificial neural networks to predict hourly electricity demand of the US cities of Fargo and Phoenix [10], and an evolutionary hybrid system which combined statistical

and machine learning techniques was used to predict the energy consumption in smart grid network installed in a residential building [11]. For improving the load demand forecasting, the artificial neural network technique was validated for short, medium, and long-term load forecasting [12], a deep learning framework was implemented to forecast electricity demand by taking care of long-term historical dependencies [13], the ensemble aggregation algorithms composed of wavelet learners were trained with a subset of selected features to execute the short-term load forecasting [14], and the uncertainty analysis of forecasting errors of PV power and load demand could be compensated by setting an adequate operating reserve (OR) [15] or treated as the dispatchable unit to cover uncertainties in load forecasting [16].

Regarding intermittent renewable energy forecasting, a deep learning-based ensemble approach was demonstrated to learn the uncertainties in wind power data [17], the machine learning models of random forest (RF) and extra trees were well suited for predicting stochastic photovoltaic (PV) generation [18], and a combination of neural networks and support vector machine (SVM) could increase the reliability of wind power forecasting [19], and the Gaussian process regression (GPR) as a probability density forecasting method could handle the uncertainties in power load data in a principled manner [20]. Regarding the technological issues for the smart hybrid energy system, an optimal load dispatch of a community-based hybrid energy system using deep learning for solar power and load forecasting could reduce total cost [21], the renewable energy sources in microgrids could ensure the environmental benefits due to the low avoided social costs of carbon [22], the presence of the battery storage system in the power generation sector could reduce the operating cost and improve energy utilization of community-based hybrid energy system [23], and the variance of state-of-charge (SOC) of the battery was tested according to quantifying cumulative impacts of stochastic forecasting errors [24].

In this paper, a smart hybrid energy system (SHES) using a combination of battery, PV system, and gas/diesel engines is served as the sustainable microgrid. The SHES is operated in the grid-connected or islanded modes for a community in New York City. The proposed configurations of SHES are shown in Section 2. The predictions of load demand, PV power, and locational-based marginal pricing (LBMP) by using selected forecast models such as linear regression (LR), logistic regression (LogR), feedforward neural network (FNN), recurrent neural network (RNN), nonlinear autoregressive exogenous model (NARX), Gaussian process regression (GPR), support vector machine (SVM), random forest (RF), extreme gradient boosting (XGBoost), and long short-term memory (LSTM) are shown in Section 3. The hour-ahead and day-ahead forecasting strategy is built from Level 1 to Level 3. Notably, Level 3 shows the blending models by using proper forecast models such as NARX, LSTM, and XGBoost. The economic/environmental dispatch optimization algorithm (EEDOA) for minimizing the total operating cost or CO₂ emissions of the SHES system is shown in Section 4. In order to address the reliable electricity supply and cope with forecasting uncertainties, the loss-of-load probability (LOLP) and the operating reserve (OR) are involved in the EEDOA. The comparisons of SHES in grid-connected or islanded modes are described in Section 5. The results show that the grid-connected mode is superior to the islanded mode due to the main grid with lower LBMP.

2. Smart Hybrid Energy System

In this study, the grid-connected mode of the smart hybrid energy system (SHES) is depicted in Figure 1, where the power source is a combination of a highly efficient gas engine (P_{ge}), a diesel engine (P_{de}), a photovoltaic (PV) system (P_{pv}), an environmentally-friendly liquid battery (P_{sb}), and the main grid (P_{mg}). Notably, the DC/DC converter with prescribed efficiency (η_{con}), the DC/AC inverter with prescribed efficiency (η_{inv}), and the efficiency of the electrical generator with the prescribed efficiency (η_{ge}) are specified. Natural gas and diesel are assumed to be sufficient for the gas engine and diesel engine, respectively. The DC and AC buses are responsible for dispatching power sources to meet the load demand (P_{load}) according to capacities of devices of power and energy storage, fuel

prices, and CO₂-eq emissions. To address the off-the-grid electricity system for locations not fitted with an electricity distribution system, the islanded (standalone) mode of the SHES does not connect to the main grid. The SHES in the face of the probability of fault occurs due to the uncertainty of renewable power production, so the energy storage system (rechargeable battery) becomes a critical option by restoring the excessive renewable power and compensating for the power gap.

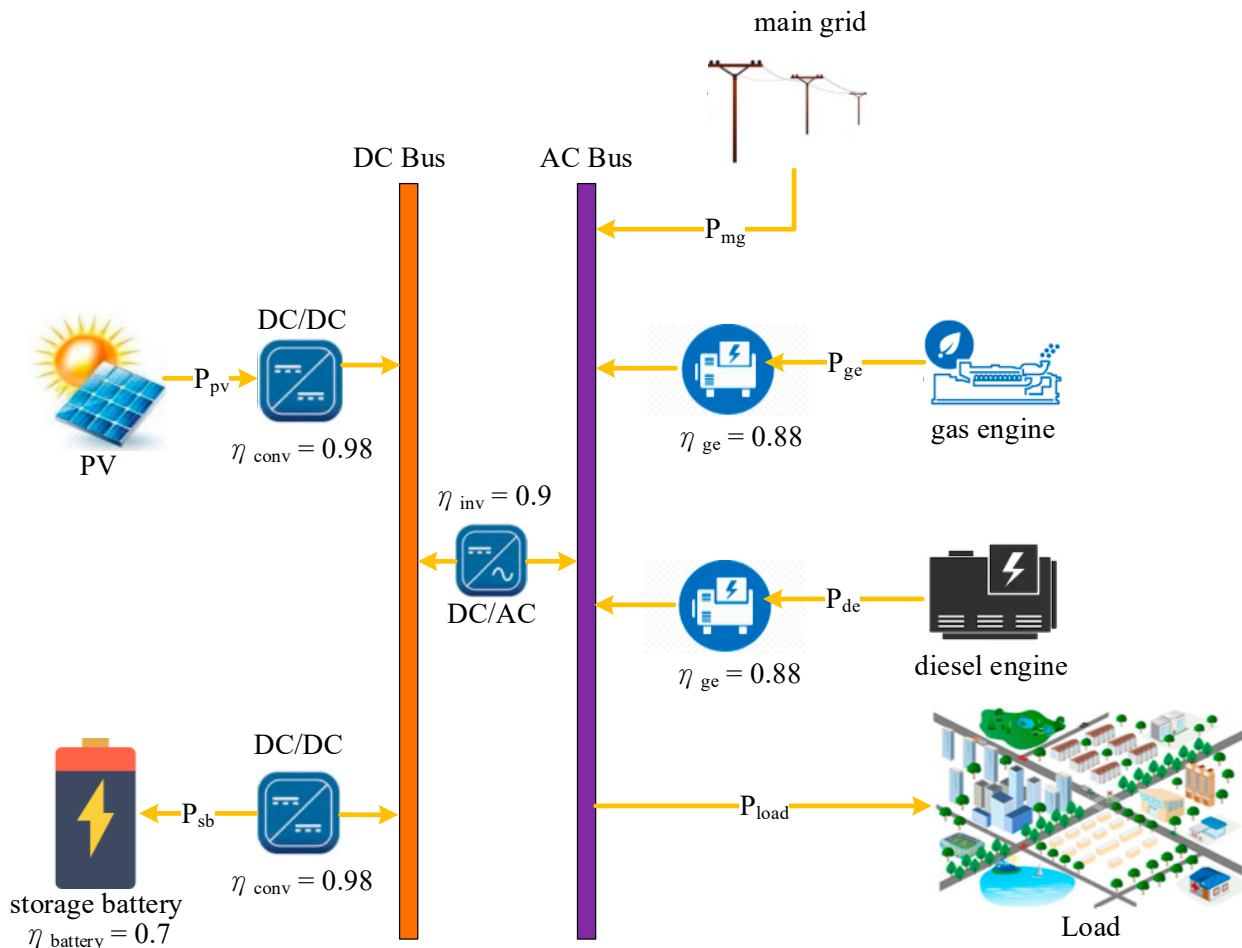


Figure 1. Schematic configuration of SHES with the grid-connected mode.

3. Forecasting

The short-term or long-term forecasting of load demand and renewable energy is a useful approach for addressing the SHES operation at lower total operating cost and greater reduction of carbon emissions. In this study, the forecasting algorithms with selected forecast models are addressed as follows.

3.1. Forecast Models

- (i) Linear regression (LR): LR is denoted as a forecast model which is directly described by

$$y_{LR} = X\beta + \varepsilon \tag{1}$$

where y_{LR} is the predicted variable, X is the input matrix, β is the parameter vector as the regression coefficient, and ε represents the error vector. The values of β are often fitted using the least-squares approach.

- (ii) Logistic regression (LogR): LogR is denoted as a forecast model in which the function is described by

$$f(x) = \beta_0 + \beta_1x_1 + \dots + \beta_nx_n \tag{2}$$

and the predicted variable y is shown by [25]

$$y_{\text{LogR}} = \delta(f(x)) = \frac{1}{1 + e^{-f(x)}} \quad (3)$$

where x_i ($i = 1, \dots, n$) is the input element, and δ represents the standard logistic function. y_{LogR} is used to model and predict categorical values through the optimization tools in Matlab®.

- (iii) Feedforward neural network (FNN): A three-layer FNN is described by [26]

$$\begin{aligned} h &= \sigma_h(W_h x + w_b) \\ y_{\text{FNN}} &= \sigma_y(W_y h + w_y) \end{aligned} \quad (4)$$

where h represents the hidden layer vector, and σ_h and σ_y are the activation functions. W_h , w_b , W_y , and w_y are undetermined weight matrices and vectors. Moreover, Bayesian optimization is utilized to adjust the parameters of the FNN model and improve the validation accuracy of FNN.

- (iv) Recurrent neural network (RNN): y_{RNN} in the discrete-time settings is described by [27]

$$\begin{aligned} h_t &= \sigma_h(W_h x_t + U_h h_{t-1} + w_b) \\ y_{\text{RNN}}|_t &= \sigma_y(W_y h_t + w_y) \end{aligned} \quad (5)$$

where U_h is additional weight. Moreover, Bayesian optimization is utilized to adjust the parameters of the RNN model and improve the validation accuracy of RNN.

- (v) Nonlinear autoregressive exogenous model (NARX): This model relates the current and past values of the time series of input and outputs as described by [28]

$$y_{\text{NARX}}|_t = f(y_{\text{NARX}}|_{t-1}, y_{\text{NARX}}|_{t-2}, \dots, u_t, u_{t-1}, \dots) + \varepsilon_t \quad (6)$$

Notably, ε_t represents the error term due to disturbances, and f is some nonlinear functions such as neural network, sigmoid function, and so on. Moreover, Bayesian optimization is implemented to optimize the hyperparameters of NARX and ensure the validation accuracy of NARX.

- (vi) Gaussian process regression (GPR): y_{GPR} is usually described by [29]

$$y_{\text{GPR}} = h(x)^T \beta + f(x) \quad (7)$$

where $h(x)$ is the explicit basis function, and $f(x) \sim \text{GP}(0, k(x, x'))$. The Gaussian process (GP) is a set of random variables, and k is the covariance matrix. Moreover, Bayesian optimization is utilized to adjust the parameters of the GPR model and improve the validation accuracy of GPR.

- (vii) Support vector machine (SVM): SVM is a supervised learning algorithm. y_{SVM} classifies data by finding the best hyperplane β [30]

$$y_{\text{SVM}} = x^T \beta + b \quad (8)$$

where β is determined by solving the following optimization algorithm

$$\min \frac{1}{2} \|\beta\|^2$$

subject to

$$\|y - y_{\text{SVM}}\| \leq \varepsilon \quad (9)$$

Moreover, Bayesian optimization is utilized to adjust the parameters of the SVM classifier and improve the validation accuracy of SVM.

- (viii) Random forest (RF) [31]: RF is an ensemble learning method for classification and regression. y_{RF} is evaluated through three steps: (i) A decision tree using all the

- features/variables of interest as an entire dataset; (ii) Bagging is used to reduce the variance of a decision tree; (iii) The random subspace method for constructing decision forests. Moreover, Bayesian optimization is utilized to adjust the parameters of the RF model and improve the validation accuracy of RF.
- (ix) Extreme gradient boosting (XGBoost) [32]: XGBoost is a decision-tree-based ensemble machine learning algorithm that uses a gradient boosting framework. y_{XGBoost} is evaluated through a combination of software and hardware optimization techniques to yield superior results using fewer computing resources in the shortest amount of time. Moreover, Bayesian optimization is utilized to adjust the parameters of XGBoost and improve the validation accuracy of XGBoost.
 - (x) Long short-term memory (LSTM): LSTM is a recurrent neural network (RNN) architecture used in the field of deep learning. y_{LSTM} is evaluated by [33]

$$\begin{aligned}
 i_t &= \sigma_h(W_i x_t + R_i h_{t-1} + b_i) \\
 f_t &= \sigma_h(W_f x_t + R_f h_{t-1} + b_f) \\
 o_t &= \sigma_h(W_o x_t + R_o h_{t-1} + b_o) \\
 \tilde{c}_t &= \tanh(W_c x_t + R_c h_{t-1} + b_c) \\
 c_t &= f_t \times c_{t-1} + i_t \times \tilde{c}_t \\
 y_{\text{LSTM}|t} = h_t &= o_t \times \tanh(c_t)
 \end{aligned} \tag{10}$$

where the matrices $R = (R_i, R_f, R_o, R_c)$, $W = (W_i, W_f, W_o, W_c)$, and $b = (b_i, b_f, b_o, b_c)$ represent weights of input, recurrent, and bias, respectively. Moreover, Bayesian optimization is implemented to optimize the hyperparameters of LSTM networks and ensure the validation accuracy of LSTM.

The forecast accuracy is validated by measuring the mean absolute scaled error (MASE)

$$\text{MASE}_j = \frac{\frac{1}{n} \sum_t |y_j|_t - A_t|}{\frac{1}{n-1} \sum_{i=2}^n |A_i - A_{i-1}|} \tag{11}$$

where $t = 1$, n is the set of forecasting sample periods. $|y_j|_t$ is the output of forecast model j at a given period t and $j = i, ii, \dots$. A_t represents the real-time value at a given period t . Notably, $n = 2$ and $n = 24$ are denoted as hour-ahead and day-ahead forecasts, respectively. The Bayesian optimization algorithm is a sequential design strategy for the global optimization of a probabilistic model of the objective function, which is available in Matlab[®].

In this study, the SHES, a class of community-based hybrid energy systems, is implemented to serve a community in New York City, where load demand, PV power, and locational-based marginal pricing (LBMP) dominate the energy management strategies. Notably, LBMP is the electricity price of the main grid, usually composed of the energy price, transmission congestion cost, and loss cost. Feasible forecasting strategies contribute to reducing greenhouse gas emissions by allocating the priorities of power units and ultimately reduce the operating costs and environmental impacts of SHES.

3.2. Forecasting Algorithm

Under the limitations of data sources at prescribed time intervals and the importance of influence, the factors for the hour-ahead and day-ahead forecasting of load demand, PV power, and LBMP are categorized with load demands of one hour, two hours, three hours, and 24 h ahead, (max/min) ambient temperatures, current ambient temperature, temperatures of the heat index, dew point, wind chill, and feels like. Moreover, the forecasting strategy is built from level 1 to level 3.

Level 1: A total of seven forecast models from (i) to (vii) are trained and validated according to selected eleven factors. The corresponding MASE of the hour-ahead and day-ahead forecast models regarding seven forecast models are shown in Tables 1 and 2,

respectively. It is noted that the forecast models of FNN, RNN, GPR, SVM, and RF could find the MASE for forecasting load demand, PV power, and LBMP at the minimum levels by using Bayesian optimization.

Table 1. Comparisons of hour-ahead forecast models of load demand, PV power, and LBMP.

Forecast Model	Load Demand (MASE)		PV Power (MASE)		LBMP (MASE)	
	Training	Validation	Training	Validation	Training	Validation
<i>Level 1</i>						
LR	1.0126	0.9467	0.8046	0.7526	0.9981	0.9043
LogR	1.0318	0.9474	0.7193	0.6930	0.9604	0.8733
FNN	0.9563	0.9062	0.4474	0.4953	0.9328	0.8504
RNN	1.0154	0.9357	0.4803	0.5000	0.9060	0.8639
GPR	0.9710	0.8965	0.4531	0.4882	0.9975	0.9042
SVM	0.9771	0.9077	0.4839	0.5060	0.8190	0.8049
RF	0.9570	0.8981	0.4352	0.5013	0.9241	0.8186
<i>Level 2</i>						
LSTM	0.9350	0.8819	0.4223	0.4790	0.9192	0.8243
XGBoost	0.9406	0.8722	0.4169	0.4860	0.8793	0.8098
<i>Level 3</i>						
Blending	0.9224	0.8664	0.4111	0.4778	0.8180	0.7985

Table 2. Comparisons of day-ahead forecast models of load demand, PV power, and LBMP.

Forecast Model	Load Demand (MASE)		PV Power (MASE)		LBMP (MASE)	
	Training	Validation	Training	Validation	Training	Validation
<i>Level 1</i>						
LR	0.8392	0.8557	1.0770	1.0780	0.7788	0.7127
LogR	0.9003	0.9094	0.6382	0.7976	0.7766	0.6980
FNN	0.7123	0.7195	0.6159	0.7613	0.8938	0.7055
RNN	0.7211	0.6920	0.6380	0.7691	0.7774	0.6988
GPR	0.8304	0.7563	0.6182	0.7692	0.7856	0.761
SVM	0.7655	0.6919	0.6504	0.7442	0.6618	0.6673
RF	0.7642	0.7649	0.5474	0.6445	0.7946	0.6866
<i>Level 2</i>						
LSTM	0.4538	0.5201	0.6786	0.6348	0.6866	0.6690
XGBoost	0.9150	0.7958	0.5436	0.6107	0.7846	0.6970
<i>Level 3</i>						
Blending	0.4081	0.5012	0.5157	0.6012	0.6515	0.6558

Level 2: Based on the same eleven factors and the outputs of seven forecast models in Level 1 for an hour-ahead forecast by using XGBoost and LSTM, the corresponding MASE of forecasting load demand, PV power, and LBMP through training and validation are shown in Table 1. It is noted that the XGBoost ensures a lower MASE than LSTM in Level 2. Based on the same factors and forecast models for the day-ahead forecast by using XGBoost and NARXNN, the corresponding MASE of day-ahead forecasting load demand, PV power, and LBMP through training and validation are shown in Table 2. It is noted that the NARXNN ensures the lowest MASE of forecasting load demand than XGBoost in Level 2, and XGBoost ensures the lowest MASE of forecasting PV power and LBMP than NARXNN in Level 2.

Level 3: Referring to a feature-weighted linear stacking method that incorporates meta-features for improved accuracy [34], the blending model adopts the information from Levels 1 and 2 to improve the prediction accuracy. The blending model by LSTM and XGBoost with prescribed coefficients (a , b , c) for the hour-ahead forecasts is shown as

$$y_{blend(1)}|_t = b(y_{LSTM}|_t)^a (y_{XGBoost}|_t)^{1-a} + c(y_{LSTM}|_t) + (1 - b - c)y_{XGBoost}|_t \quad (12)$$

Similarly, the blending model by NARX and XGBoost with prescribed coefficients (α , β , γ) for the day-ahead forecast is shown as

$$y_{blend(2)} \Big|_t = \beta (y_{NARX} \Big|_t)^\alpha (y_{XGBoost} \Big|_t)^{1-\alpha} + \gamma (y_{NARX} \Big|_t + (1 - \beta - \gamma) y_{XGBoost} \Big|_t) \quad (13)$$

Notably, these coefficients in Equations (11) and (12) are determined by minimizing MASE of forecasting load demand, PV power, and LBMP using Bayesian optimization. Moreover, the forecast strategies from Level 1 to Level 3 are described by a flowchart which is shown in Figure S1 in Supplementary Materials. Based on the hour-ahead and day-ahead forecasts in Tables 1 and 2, the blending model could ensure the lowest MASE of forecasting load demand, PV power, and LBMP than other models used in Levels 1 and 2.

The comparisons of the hour-ahead and day-ahead forecasting performances of load demand, PV power, and LBMP are shown in Figure 2a–c, respectively. By using the blending models for hour-ahead and day-ahead forecasting, Figure 2a shows that the hour-ahead load demand forecasting is superior to the day-ahead load demand forecasting as compared to the real-time data of load demand, Figure 2b shows that the hour-ahead PV power forecasting is superior to the day-ahead PV power forecasting as compared the real-time data of PV power, and Figure 2c shows that the hour-ahead LBMP forecasting is superior to the day-ahead LBMP forecasting as compared the real-time data of LBMP. Notably, the day-ahead load demand forecasting fails when they exceed 18 h, and the hour-ahead and day-ahead LBMP forecastings are not qualified, while two LBMP peaks appear at specific periods.

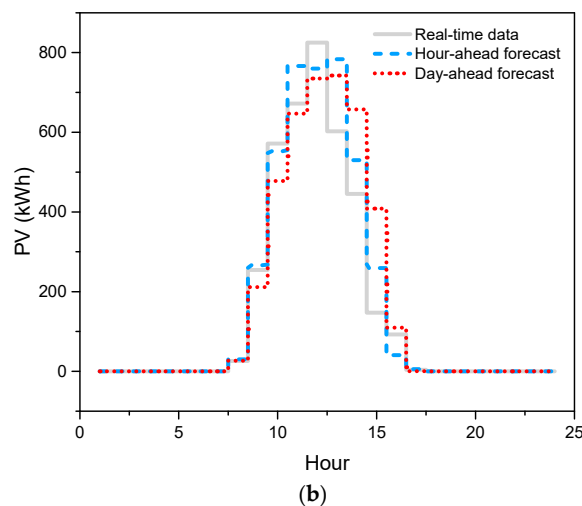
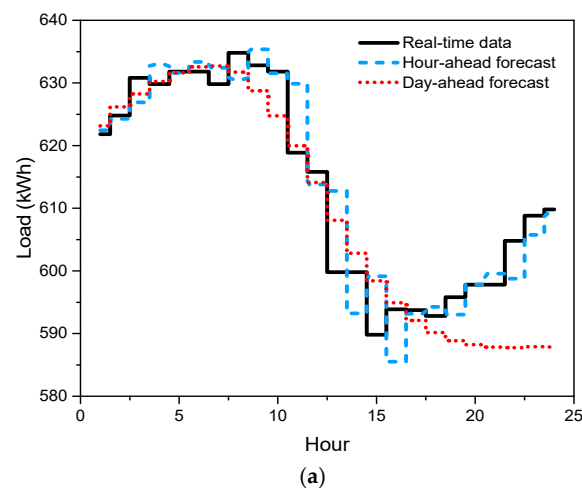


Figure 2. Cont.

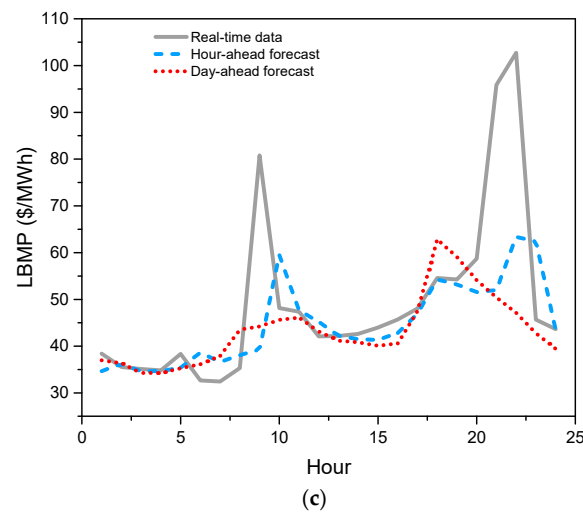


Figure 2. Comparisons of hour-ahead and day-ahead forecasts and real-time data w.r.t. (a) load demand, (b) PV power, and (c) locational-based marginal pricing (LBMP).

4. Optimal Power Dispatch Strategy

The priority of power supplies according to the intermittent energy source, carbon emissions, and fuel/electricity prices is taken into consideration to address the optimal power dispatch strategy for the SHES. In this approach, the PV power is the priority unit due to free solar energy and zero emissions, and the battery is the second priority unit to cope with the power gap and meet the limits of the state of charge (SOC) of the battery simultaneously; the gas engine or diesel engine or main grid is the third priority unit to achieve the cost balancing among parallel energy sources.

4.1. Operating Reserve

The operating reserve (OR) is added to compensate imbalance between load demand and power supplies and the unpredictable imbalance due to the forecasting uncertainties. For the assessment of forecasting uncertainty, the normal probability density function (*npdf*) is shown by [15]

$$npdf(\varepsilon) = \frac{1}{\sigma\sqrt{2\pi}} e^{-\frac{(\varepsilon-\mu)^2}{2\sigma^2}} \quad (14)$$

where ε represents the forecasting errors of load demand (ε_L^t) and PV power (ε_{PV}^t). Both forecasting errors are expressed by

$$\varepsilon_L^t = L_A^t - L_F^t \quad (15)$$

$$\varepsilon_{PV}^t = PV_A^t - PV_F^t \quad (16)$$

where L_A^t and L_F^t represent the real-time and forecasting load demand at a time period t , respectively. Similarly, PV_A^t and PV_F^t represent the real-time and forecasting PV power at a time period t , respectively. The first *npdf* of the forecasting errors of load demand and PV power is specified to address the operating reserve quantification. Second, the forecasting error of net demand (ε_{ND}^t) is described by

$$\varepsilon_{ND}^t = ND_A^t - ND_F^t \quad (17)$$

and

$$ND_A^t = L_A^t - PV_A^t \times \eta_{con} \times \eta_{inv} \quad (18)$$

$$ND_F^t = L_F^t - PV_F^t \times \eta_{con} \times \eta_{inv} \quad (19)$$

where ND_A^t and ND_F^t represent the net real-time and net forecasting load demand at a time period t , respectively. η_{con} and η_{inv} represent the efficiencies of the converter and inverter, respectively. Third, the loss-of-load probability (LOLP) or risk is specified where the LOLP is expressed by

$$LOLP = \sum_{t=1}^n Pr(\varepsilon_{ND}^t > 0) \quad (20)$$

where $Pr(\varepsilon_{ND}^t > 0)$ represents the probability of ND_F^t while $\varepsilon_{ND}^t > 0, t = 1, 2, \dots, 24$.

For accessing the forecasting uncertainty at 12 o'clock ($t = 12$), Figure 3a,b shows that the forecasting errors of load demand and PV power are symmetric probability distributions, respectively. By Equations (17)–(20), the probability distributions of net load demand (ε_{ND}^t) is depicted in Figure 3c, notably the green part while $\varepsilon_{ND}^t > 0$ is adjusted to evaluate LOLP. Through the inverse of the normal cumulative distribution function of ND_F^t , the daily OR^t with 5~30% of LOLP is obtained, which is depicted in Figure 4a. It is noted that the higher LOLP implies a lower OR^t. Figure 4b shows the profile of OR ($t = 12$ h) vs. LOLP; notably, in this study, OR ($t = 12$ h) is determined at the accepted risk (LOLP) with 10%.

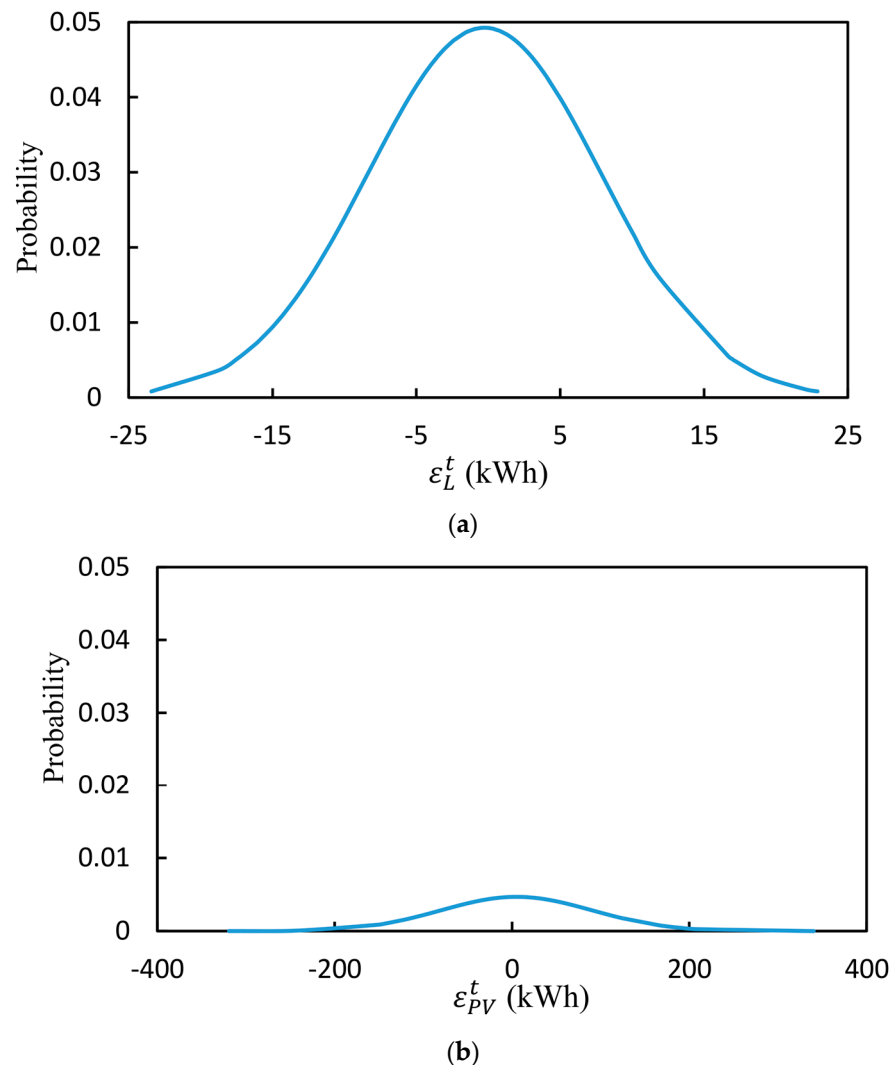


Figure 3. Cont.

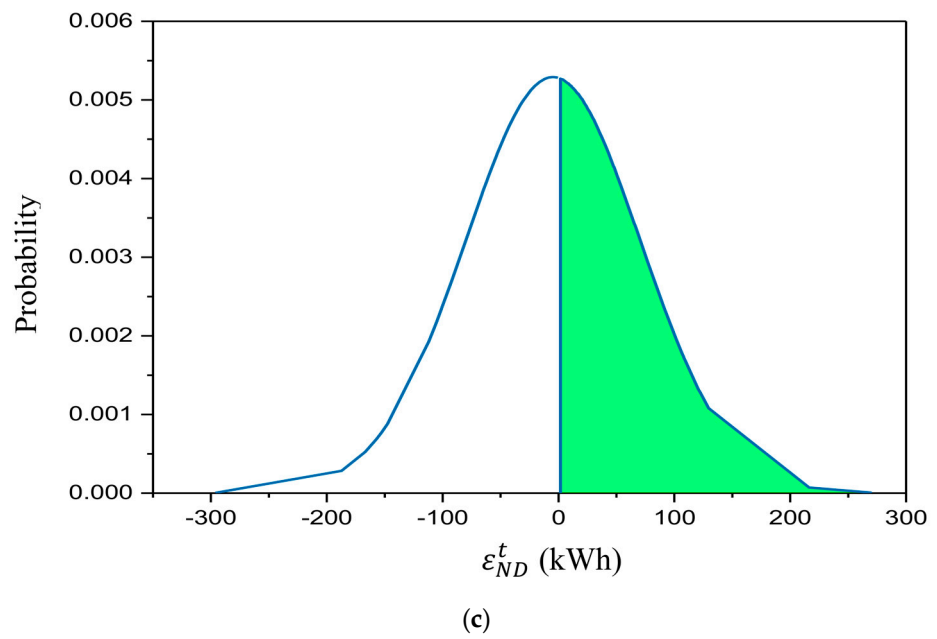


Figure 3. Probability vs. forecasting errors of (a) load demand (ϵ_L^t), (b) PV power (ϵ_{PV}^t), and (c) netload demand (ϵ_{ND}^t)

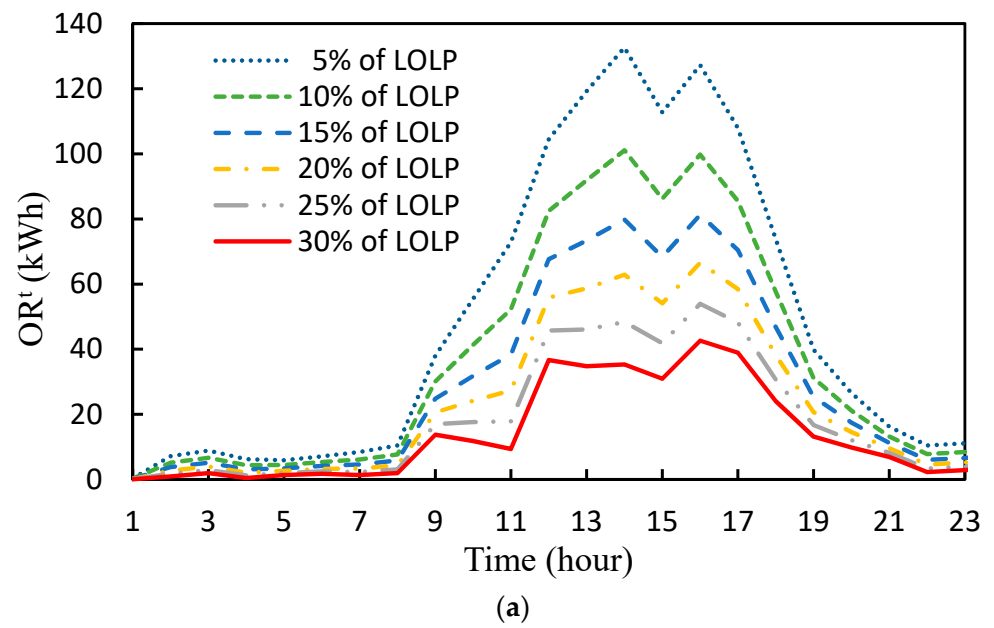


Figure 4. Cont.

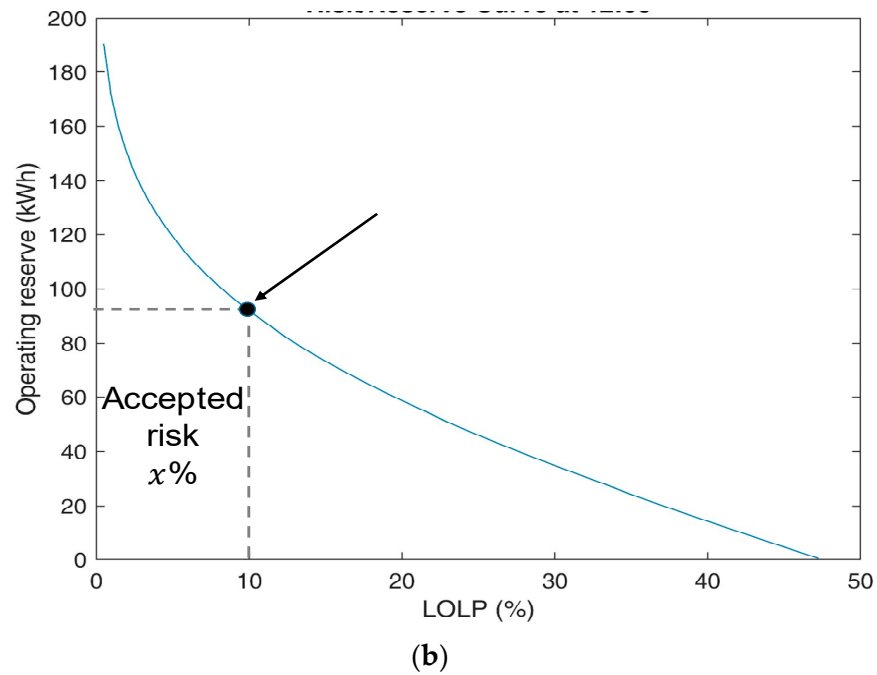


Figure 4. Operating reserve: (a) OR^t vs. 24 h and (b) OR vs. LOLP.

4.2. Optimization

The economic/environmental dispatch optimization algorithm (EEDOA) is described as follows.

$$\min_{P_{ge}^t, P_{de}^t, P_{mg}^t} \{wC_T + (1 - w)\lambda E_T\} \tag{21}$$

Subject to

(i) The grid-connected mode:

$$(P_{ge}^t + P_{de}^t) \times \eta_{ge} + (P_{sb}^t + PV_F^t) \times \eta_{con} \times \eta_{inv} + P_{mg}^t - (L_F^t + OR^t) = 0, \text{ if } P_{sb}^t > 0 \tag{22}$$

$$(P_{ge}^t + P_{de}^t) \times \eta_{ge} + PV_F^t \times \eta_{con} \times \eta_{in} + P_{sb}^t \times \frac{\eta_{inv}}{\eta_{con}} + P_{mg}^t - (L_F^t + OR^t) = 0, \text{ if } P_{sb}^t < 0 \tag{23}$$

Or The islanded mode:

$$(P_{ge}^t + P_{de}^t) \times \eta_{ge} + (P_{sb}^t + PV_F^t) \times \eta_{con} \times \eta_{inv} - (L_F^t + OR^t) = 0, \text{ if } P_{sb}^t > 0 \tag{24}$$

$$(P_{ge}^t + P_{de}^t) \times \eta_{ge} + PV_F^t \times \eta_{con} \times \eta_{in} + P_{sb}^t \times \frac{\eta_{inv}}{\eta_{con}} - (L_F^t + OR^t) = 0, \text{ if } P_{sb}^t < 0 \tag{25}$$

(ii) The upper and lower bounds of power units

$$P_{ge,min} < P_{ge}^t < P_{ge,max} \tag{26}$$

$$P_{de,min} < P_{de}^t < P_{de,max} \tag{27}$$

$$P_{sb,min} < P_{sb}^t < P_{sb,max} \tag{28}$$

In Equation (21), the conflicting objectives are converted into a single goal with weight coefficients w and λ , C_T represents the total operating cost (\$/kWh) of the SHES, which includes the price of main grid electricity and operating costs by using the power of the gas engine and diesel engine, and E_T represents the total CO₂ emissions (kg CO₂-eq/kWh) which involve CO₂ emissions from the gas engine, diesel engine, and main grid. In Equations (22)–(25), OR^t can be found if LOLP is fixed at 10% in Figure 4a, and the hour-ahead forecasting of load demand and PV power can be found in Figure 2a,b.

According to average prices in December 2018 from the U.S. Energy Information Administration (EIA) [35], the fuel prices of natural gas and diesel are given at 0.412 \$/m³ and 0.888 \$/L, respectively. According to the information from the New York Independent System Operator (NYISO) [36], the floating grid price (C_{mg}) is determined by max{LBMP, 5 \$/MWh}. Assumed that the maximum power outputs of the gas engine and diesel engine are set as $P_{ge,max} = 250$ kWh and $P_{de,max} = 648$ kWh, respectively, the operating costs of the gas engine and diesel engine are obtained according to the following regression models

$$C_{NG} = 0.412 \times \left(17.35 + 0.2184 \times P_{ge}^i + 0.0002688 \times \left(P_{ge}^i \right)^2 \right) \quad (29)$$

$$C_{diesel} = 0.888 \times \left(13 + 0.2088496 P_{de}^i + 0.0000192 \left(P_{de}^i \right)^2 \right) \quad (30)$$

Moreover, the total operating cost (C_T) of the SHES is described by

$$C_T = \sum_{i=1}^n C_{NG}^i + C_{diesel}^i + C_{mg}^i \quad (31)$$

According to the IPCC 2013 100-year GWP report by using SimaPro[®], CO₂ emissions of gas engines, diesel engines, and main grid are 0.738 kgCO₂-eq/kWh, 1.138 kgCO₂-eq/kWh, and 0.788 kg CO₂-eq/kWh, respectively. Moreover, the total CO₂ emissions (E_T) of the SHES are described by

$$E_T = \sum_{i=1}^n 0.738 \times P_{ge}^i + 1.138 \times P_{de}^i + 0.788 \times P_{mg}^i \quad (32)$$

For the islanded mode of SHES with the prescribed period, C_{mg}^i and P_{mg}^i are removed from two objectives in Equations (31) and (32), respectively. The state of charge (SOC) of the battery for the grid-connected and islanded modes is described by

$$\text{SOC}(t) = \text{SOC}(t-1) + (P_{sb}^t / E_c) \times \eta_d^{-1}, \text{ if } P_{sb}^t > 0 \quad (33)$$

$$\text{SOC}(t) = \text{SOC}(t-1) + (P_{sb}^t / E_c) \times \eta_c, \text{ if } P_{sb}^t < 0 \quad (34)$$

where η_d and η_c represent the discharging and charging efficiencies of the battery, respectively. E_c represents the fixed battery capacity.

5. Results and Discussion

First, the accepted risk or LOLP is fixed at 10%, and OR^t can be found in Figure 4b, the SHES of efficiencies with $\eta_{con} = 0.98$ and $\eta_{inv} = 0.88$ are specified, and the minimum power outputs of the gas engine and diesel engine are set with $P_{ge,min} = P_{de,min} = 0$. Second, the specifications of rechargeable batteries include battery efficiencies with $\eta_d = \eta_c = 0.7$, the battery capacity with $E_c = 2400$ kW, and the operating bounds of charge and discharge of rechargeable battery between $P_{sb,min} = -1000$ kWh and $P_{sb,max} = 750$ kWh. Third, the EEDOA with specified w is solved by using a GAMS[®] solver named the Branch-and-Reduce Optimization Navigator (BARON) [37]. Notably, the EEDOA with $w = 1$ is treated as the economic dispatch optimization problem, and the EEDOA with $w = 0$ becomes the environmental dispatch optimization problem. Moreover, the optimal dispatching of a smart hybrid energy system via uncertainty analysis, operating reserve, and hour-ahead and day-ahead forecasting strategies described by a flowchart are shown in Figure 5.

5.1. Daily Forecasting Comparisons

In order to meet the real-time daily load demand, the economic/environmental power dispatch strategies for the grid-connected and islanded modes of SHES by solving EEDOA are shown in Figure 6a,c and Figure 7a,c, respectively.

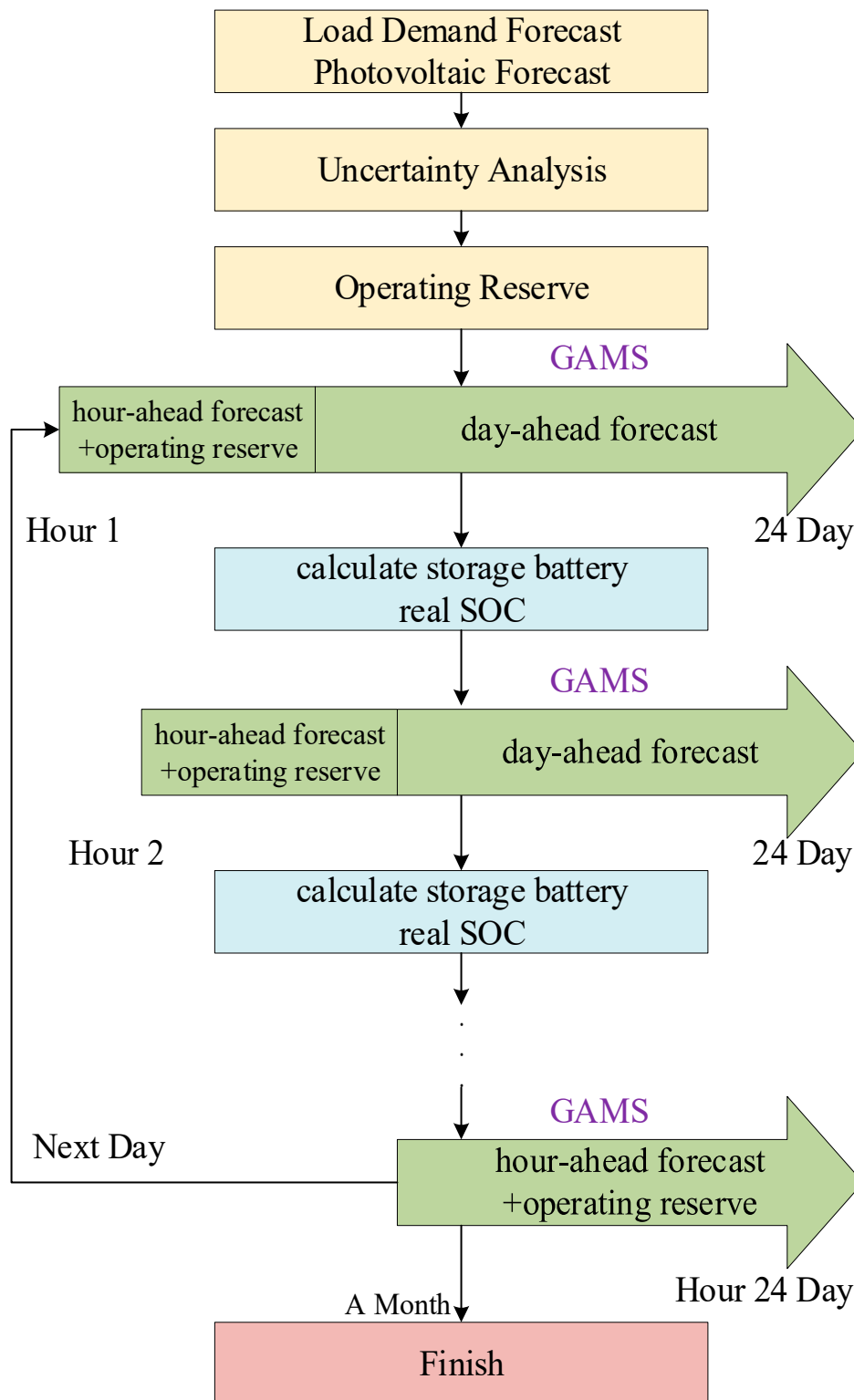


Figure 5. Flow chart for optimal dispatching of smart hybrid energy system via uncertainty analysis, operating reserve, and hour-ahead and day-ahead forecasting strategies.

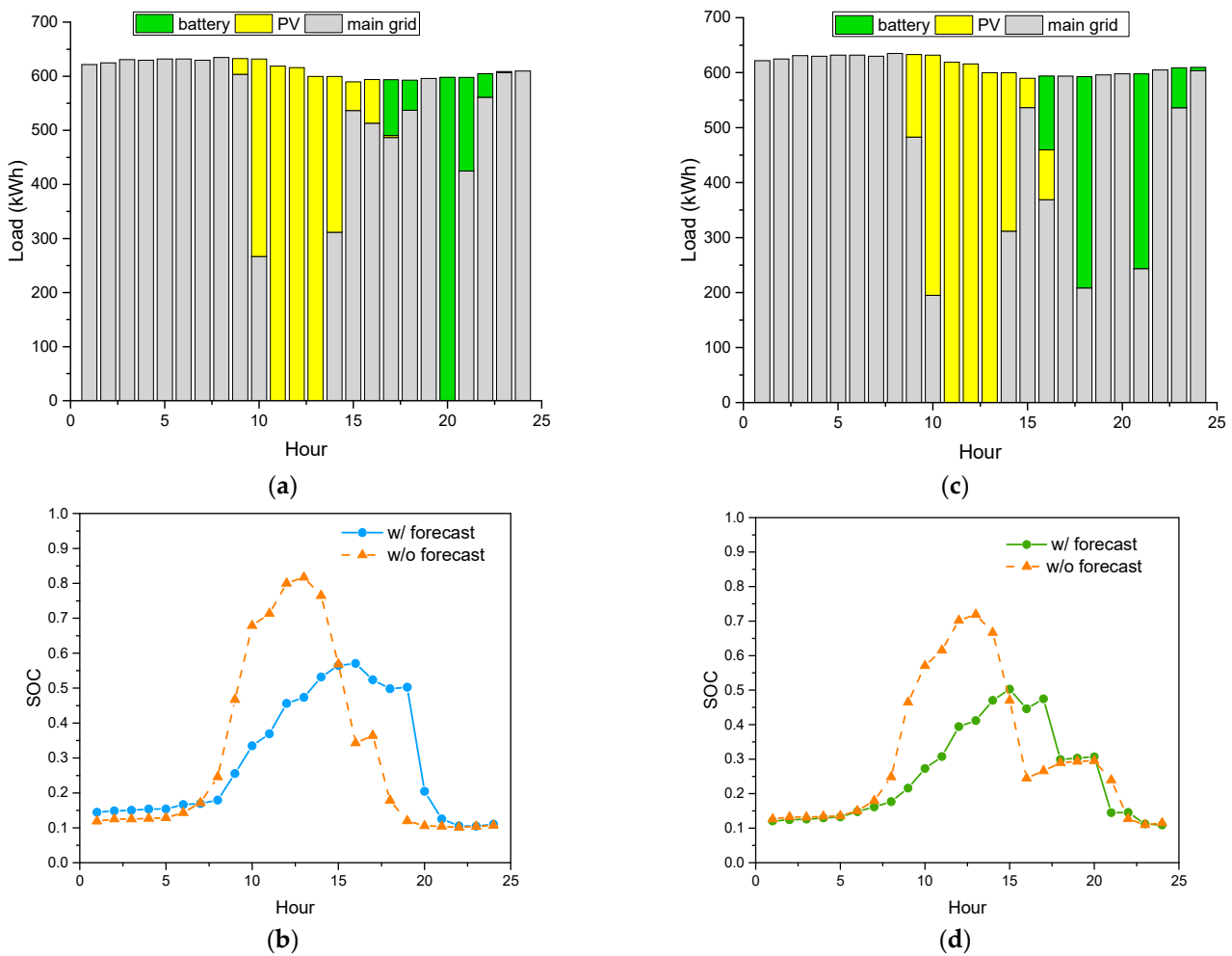


Figure 6. The grid-connected mode of SHES using economic dispatching by showing (a) power dispatch stacking and (b) SOC responses for one day and using environment dispatching by showing (c) power dispatch stacking and (d) SOC responses for one day.

- (a) In the grid-connected mode, the main grid (gray bar) in Figure 6a,c dominates the main power supply due to limits of energy storage capacity and intermittent solar energy. Due to the main grid with lower LBMP, conventional gas/diesel engines are absent. Using the environmental dispatch strategy by solving EEDO with $w = 0$, the power supply from the battery shown in Figure 6c is higher than in Figure 6a, such that the corresponding SOC in Figure 6d is lower than in Figure 6b.
- (b) In the islanded mode, the gas turbine (orange bar) and diesel engine (gray bar) in Figure 7a,c become the main power supplies due to no main grid. Using the economic dispatch strategy by solving EEDO with $w=1$, the diesel consumption (diesel engine) in Figure 7a is higher than in Figure 7c, such that the corresponding SOC in Figure 7b is higher than in Figure 7d.

In the grid-connected mode, the lower bounds of SOC in Figure 6b,d can maintain over 0.1; notably, the power dispatch with a forecast can reduce the upper bounds of SOC as compared to the power dispatch without a forecast. In the islanded mode, the power dispatch with a forecast can reduce the upper bounds of SOC as compared to the power dispatch without a forecast, but it may induce a very low battery (close to 0) risk during a period of one day as shown in Figure 7b,d. It is noted that the hour-ahead forecast power dispatch strategy can reduce QR and decrease operating costs.

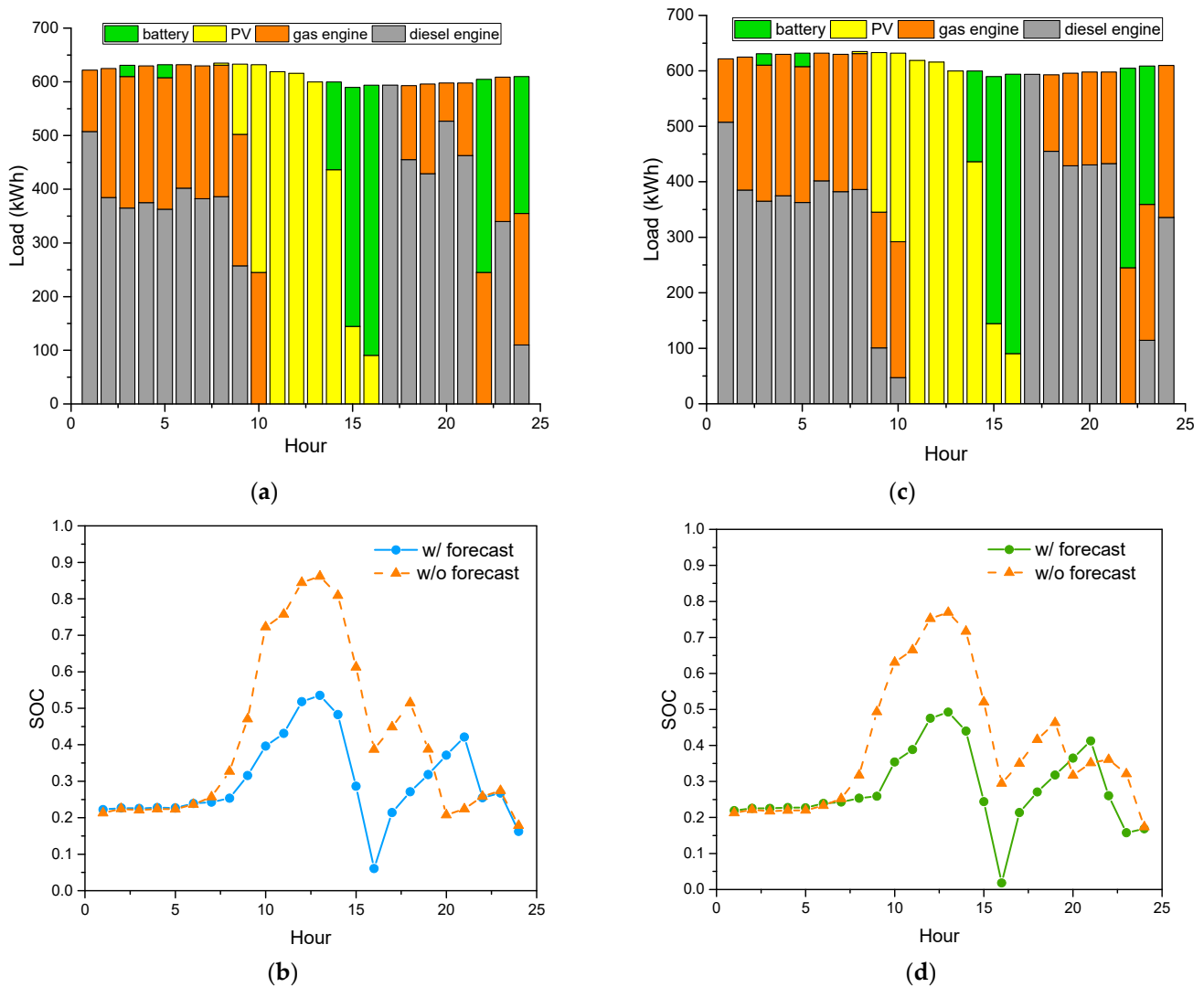


Figure 7. The islanded mode of SHES using economic dispatching by showing (a) power dispatch stacking and (b) SOC responses for one day and using environment dispatching by showing (c) power dispatch stacking and (d) SOC responses for one day.

5.2. Monthly Forecasting Comparisons

In order to meet the real-time monthly load demand, the economic/environmental power dispatch strategies for the grid-connected and islanded modes of SHES by solving EEDOA are addressed, and the corresponding SOC of the battery is shown in Figure 8a–d. These figures show that the day-ahead forecast power dispatch strategy can reduce the upper bounds of SOC as compared to the power dispatch without forecast. Similarly, the day-ahead forecast power dispatch strategy may induce a very low battery (close to 0) risk during a period of one month. It is verified that the power dispatch for the grid-connected and islanded modes of SHES using the long-term forecasting algorithm is feasible.

Moreover, Table 3 shows that the forecast-based economic dispatch optimization strategy can reduce the monthly operating costs (C_T) of SHES in both modes by 1.8~6.1% as compared to it without the use of forecast methods, and the forecast-based environmental dispatch optimization strategy can reduce the monthly CO_2 -eq emissions (E_T) of SHES in both modes by 1.9~5.1% as compared to it without the use of forecast methods. Notably, the monthly operating costs of the grid-connected mode are lower than the islanded mode by 72.6%. From the economic aspect, the grid-connected mode of SHES is superior to the islanded mode of HMG.

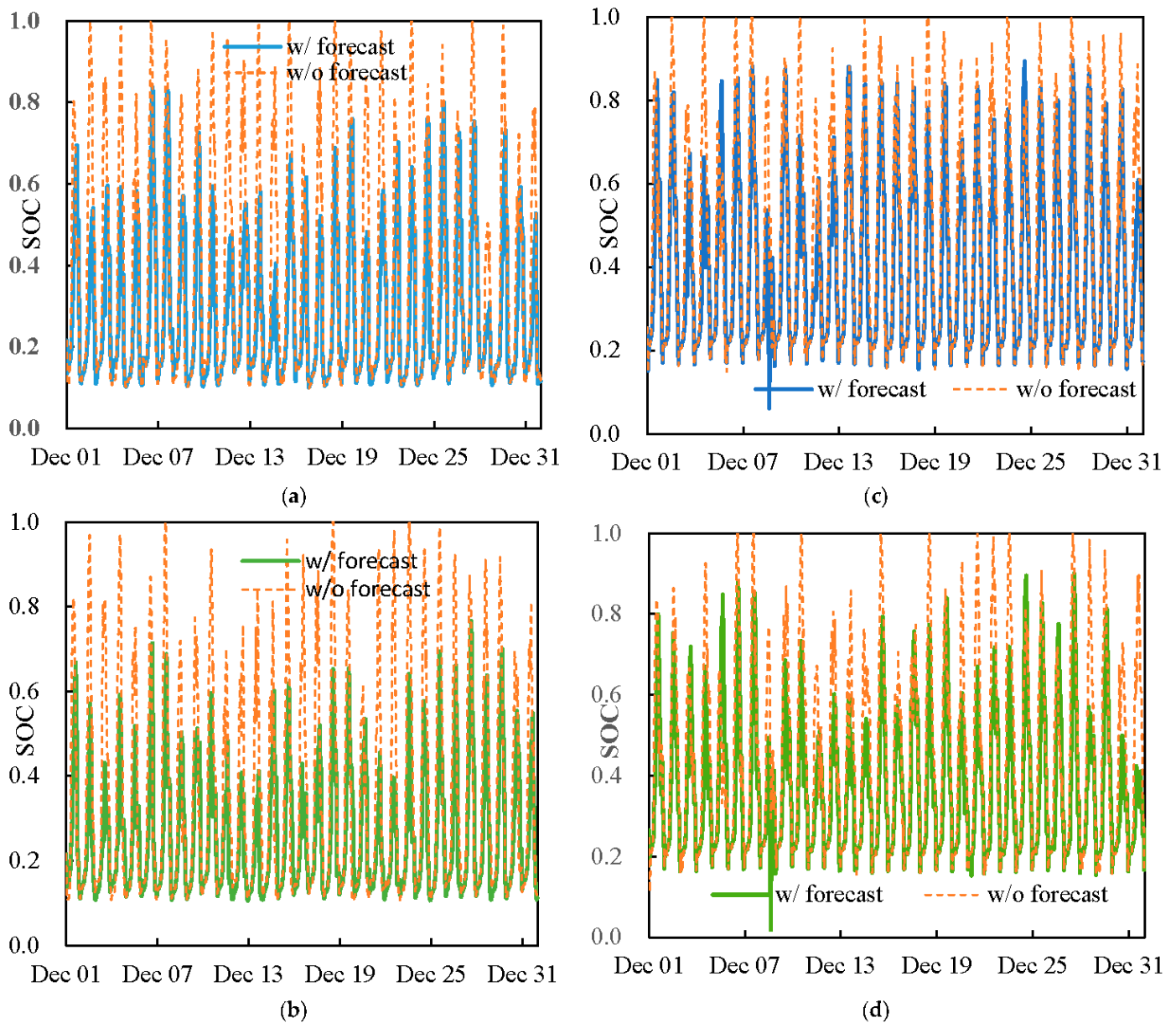


Figure 8. SOC responses for one month: (a) the grid mode of SHES using economic dispatching, (b) the grid mode of SHES using environment dispatching, (c) the islanded mode of SHES using economic dispatching, and (d) the islanded mode of SHES using environment dispatching.

Table 3. The grid-connected and islanded modes w.r.t. total operating cost and CO₂-eq emissions.

Evaluation	EEDOA	Economic Dispatch Optimization		Environmental Dispatch Optimization	
		Forecast	No Forecast	Forecast	No Forecast
Grid-connected mode					
C _T \$/mon		18,589.21	19,061.08	21,578.47	21,956.97
E _T kg/mon		404,914.61	412,465.08	403,682.54	412,028.02
Islanded mode					
C _T \$/mon		74,991.03	79,087.03	78,639.83	83,427.78
E _T kg/mon		416,585.41	437,626.21	413,979.07	433,580.64

6. Conclusions

The power dispatch of the grid-connected and islanded modes of SHES, according to the forecast-assisted EEDOA, is successfully addressed. Through the training and test of the forecasting strategy from Level 1 to Level 3, the blending model by using LSTM and XGBoost is validated to effectively improve the prediction accuracy. Accounting for the loss-of-load probability and the operating reserve in the EEDOA, the simulations show that both modes of SHES not only keep feasibility but also the monthly operating costs of SHES are reduced by 1.8~6.1%, and the corresponding monthly CO₂-eq emissions are reduced by 1.9~5.1% when the forecasting strategy is taken into account. To address the low total operating cost or total CO₂-eq emissions for SHES, gas/diesel engines play a key role in the SHES.

Supplementary Materials: The following supporting information can be downloaded at: <https://www.mdpi.com/article/10.3390/en16093698/s1>, Figure S1: Flowchart of forecasting process from Level 1 to Level 3.

Author Contributions: Conceptualization, W.W. and K.V.; Methodology, S.-C.C.; Validation, S.-C.C.; Investigation, S.-C.C.; Writing—original draft, W.W.; Writing—review & editing, K.V.; Supervision, W.W. All authors have read and agreed to the published version of the manuscript.

Funding: This research was funded by National Science and Technology Council, Taiwan grant number 108-2221-E-006-151.

Acknowledgments: We would like to thank Wei-Chen Chang for providing useful suggestions and figures. This work was financially supported by the National Science and Technology Council, Taiwan, under Grant 108-2221-E-006-151.

Conflicts of Interest: The authors declare no conflict of interest.

Nomenclature

EEDOA	Economic/environmental dispatch optimization algorithm
FNN	Feedforward neural network
GPQR	Gaussian process quantile regression
GPR	Gaussian process regression
LBMP	Locational-based marginal pricing
LOLP	Loss-of-load probability
LogR	Logistic regression
LR	Linear regression
LSTM	Long short-term memory
MASE	Mean absolute scaled error
NARX	Nonlinear autoregressive exogenous model
OR	Operating reserve
RF	Random forest
RNN	Recurrent neural network
SHES	Smart hybrid energy system
SVM	Support vector machine
SOC	State-of-charge
XGBoost	Extreme gradient boosting
C_T	Total operating cost, \$/kWh
C_{NG}, C_{diesel}	operating costs of gas engine and diesel engines, respectively, \$/kWh
P_{ge}	Gas engine power, kWh
P_{de}	Diesel engine power, kWh
P_{sb}	Rechargeable battery, kWh
P_{mg}	Main grid, kWh

η_{con}	Converter efficiency, %
η_{inv}	Inverter efficiency, %
η_{ge}	Electrical generator efficiency, %
β	Regression coefficient
δ	Standard logistic function
σ_h, σ_y	Activation functions in hidden layer and output layer, respectively
W_h, w_b, W_y, w_y	Weights in FNN and RNN
$npdf$	Normal probability density function
$\varepsilon_L, \varepsilon_{PV}$	Forecasting errors of load demand and PV power, respectively, kWh
L_A, L_F	Real-time and forecasting load demand, respectively, kWh
ND_A, ND_F	Net real-time and net forecasted demand, respectively, kWh
P_r	Probability

References

- Bartolini, A.; Carducci, F.; Muñoz, C.B.; Comodi, G. Energy Storage and Multi Energy Systems in Local Energy Communities with High Renewable Energy Penetration. *Renew. Energy* **2020**, *159*, 595–609. [\[CrossRef\]](#)
- Gil, G.O.; Chowdhury, J.I.; Balta-Ozkan, N.; Hu, Y.; Varga, L.; Hart, P. Optimising Renewable Energy Integration in New Housing Developments with Low Carbon Technologies. *Renew. Energy* **2021**, *169*, 527–540. [\[CrossRef\]](#)
- Groppi, D.; Astiaso Garcia, D.; LoBasso, G.; DeSantoli, L. Synergy between Smart Energy Systems Simulation Tools for Greening Small Mediterranean Islands. *Renew. Energy* **2019**, *135*, 515–524. [\[CrossRef\]](#)
- Chen, X.; Xiao, J.; Yuan, J.; Xiao, Z.; Gang, W. Application and Performance Analysis of 100% Renewable Energy Systems Serving Low-Density Communities. *Renew. Energy* **2021**, *176*, 433–446. [\[CrossRef\]](#)
- Zia, M.F.; Elbouchikhi, E.; Benbouzid, M. Microgrids Energy Management Systems: A Critical Review on Methods, Solutions, and Prospects. *Appl. Energy* **2018**, *222*, 1033–1055. [\[CrossRef\]](#)
- Liu, Z.; Zhang, H.; Dong, J.; Yu, H. A Prediction-Based Optimization Strategy to Balance the Use of Diesel Generator and Emergency Battery in the Microgrid. *Int. J. Energy Res.* **2020**, *44*, 5425–5440. [\[CrossRef\]](#)
- Osório, G.J.; Lujano-Rojas, J.M.; Matias, J.C.O.; Catalão, J.P.S. A Probabilistic Approach to Solve the Economic Dispatch Problem with Intermittent Renewable Energy Sources. *Energy* **2015**, *82*, 949–959. [\[CrossRef\]](#)
- Khan, N.A.; Sidhu, G.A.S.; Awan, A.B.; Ali, Z.; Mahmood, A. Modeling and Operation Optimization of RE Integrated Microgrids Considering Economic, Energy, and Environmental Aspects. *Int. J. Energy Res.* **2019**, *43*, 6721–6739. [\[CrossRef\]](#)
- Karim, M.A.; Currie, J.; Lie, T.T. A Machine Learning Based Optimized Energy Dispatching Scheme for Restoring a Hybrid Microgrid. *Electr. Power Syst. Res.* **2018**, *155*, 206–215. [\[CrossRef\]](#)
- Nagapurkar, P.; Smith, J.D. Techno-Economic Optimization and Social Costs Assessment of Microgrid-Conventional Grid Integration Using Genetic Algorithm and Artificial Neural Networks: A Case Study for Two US Cities. *J. Clean. Prod.* **2019**, *229*, 552–569. [\[CrossRef\]](#)
- Izidio, D.M.; de Mattos Neto, P.S.; Barbosa, L.; de Oliveira, J.F.; Marinho, M.H.; Rissi, G.F. Evolutionary Hybrid System for Energy Consumption Forecasting for Smart Meters. *Energies* **2021**, *14*, 1794. [\[CrossRef\]](#)
- Xia, C.; Wang, J.; McMenemy, K. Short, Medium and Long Term Load Forecasting Model and Virtual Load Forecaster Based on Radial Basis Function Neural Networks. *Int. J. Electr. Power Energy Syst.* **2010**, *32*, 743–750. [\[CrossRef\]](#)
- Bedi, J.; Toshniwal, D. Deep Learning Framework to Forecast Electricity Demand. *Appl. Energy* **2019**, *238*, 1312–1326. [\[CrossRef\]](#)
- Ribeiro, G.T.; Mariani, V.C.; dos Santos Coelho, L. Enhanced Ensemble Structures Using Wavelet Neural Networks Applied to Short-Term Load Forecasting. *Eng. Appl. Artif. Intell.* **2019**, *82*, 272–281. [\[CrossRef\]](#)
- Yan, X.; Abbes, D.; Francois, B. Uncertainty Analysis for Day Ahead Power Reserve Quantification in an Urban Microgrid Including PV Generators. *Renew. Energy* **2017**, *106*, 288–297. [\[CrossRef\]](#)
- Alvarado-Barrios, L.; Rodríguez del Nozal, Á.; Boza Valerino, J.; García Vera, I.; Martínez-Ramos, J.L. Stochastic Unit Commitment in Microgrids: Influence of the Load Forecasting Error and the Availability of Energy Storage. *Renew. Energy* **2020**, *146*, 2060–2069. [\[CrossRef\]](#)
- Wang, H.Z.; Li, G.Q.; Wang, G.B.; Peng, J.C.; Jiang, H.; Liu, Y.T. Deep Learning Based Ensemble Approach for Probabilistic Wind Power Forecasting. *Appl. Energy* **2017**, *188*, 56–70. [\[CrossRef\]](#)
- Ahmad, M.W.; Mourshed, M.; Rezgui, Y. Tree-Based Ensemble Methods for Predicting PV Power Generation and Their Comparison with Support Vector Regression. *Energy* **2018**, *164*, 465–474. [\[CrossRef\]](#)
- Wang, G.; Jia, R.; Liu, J.; Zhang, H. A Hybrid Wind Power Forecasting Approach Based on Bayesian Model Averaging and Ensemble Learning. *Renew. Energy* **2020**, *145*, 2426–2434. [\[CrossRef\]](#)
- Yang, Y.; Li, S.; Li, W.; Qu, M. Power Load Probability Density Forecasting Using Gaussian Process Quantile Regression. *Appl. Energy* **2018**, *213*, 499–509. [\[CrossRef\]](#)
- Wen, L.; Zhou, K.; Yang, S.; Lu, X. Optimal Load Dispatch of Community Microgrid with Deep Learning Based Solar Power and Load Forecasting. *Energy* **2019**, *171*, 1053–1065. [\[CrossRef\]](#)

22. Parag, Y.; Ainspan, M. Sustainable Microgrids: Economic, Environmental and Social Costs and Benefits of Microgrid Deployment. *Energy Sustain. Dev.* **2019**, *52*, 72–81. [[CrossRef](#)]
23. Moradi, H.; Esfahanian, M.; Abtahi, A.; Zilouchian, A. Optimization and Energy Management of a Standalone Hybrid Microgrid in the Presence of Battery Storage System. *Energy* **2018**, *147*, 226–238. [[CrossRef](#)]
24. Chen, Y.; Deng, C.; Li, D.; Chen, M. Quantifying Cumulative Effects of Stochastic Forecast Errors of Renewable Energy Generation on Energy Storage SOC and Application of Hybrid-MPC Approach to Microgrid. *Int. J. Electr. Power Energy Syst.* **2020**, *117*, 105710. [[CrossRef](#)]
25. Logistic Regression—A Complete Tutorial with Examples in R. Available online: <https://www.machinelearningplus.com/machine-learning/logistic-regression-tutorial-examples-r/> (accessed on 20 June 2022).
26. Deep Learning: Feed Forward Neural Networks (FFNNs) by Mohammed Terry-Jack Medium. Available online: <https://medium.com/@b.terryjack/introduction-to-deep-learning-feed-forward-neural-networks-ffnns-a-k-a-c688d83a309d> (accessed on 20 June 2022).
27. Simple Explanation of Recurrent Neural Network (RNN) by Omar Boufeloussen The Startup Medium. Available online: <https://medium.com/swlh/simple-explanation-of-recurrent-neural-network-rnn-1285749cc363> (accessed on 20 June 2022).
28. Boussaada, Z.; Curea, O.; Remaci, A.; Camblong, H.; Bellaaj, N.M. A Nonlinear Autoregressive Exogenous (NARX) Neural Network Model for the Prediction of the Daily Direct Solar Radiation. *Energies* **2018**, *11*, 11030620. [[CrossRef](#)]
29. Schulz, E.; Speekenbrink, M.; Krause, A. A Tutorial on Gaussian Process Regression: Modelling, Exploring, and Exploiting Functions. *J. Math. Psychol.* **2018**, *85*, 1–16. [[CrossRef](#)]
30. Smola, A.J.; Schölkopf, B. A Tutorial on Support Vector Regression. *Stat. Comput.* **2004**, *14*, 199–222. [[CrossRef](#)]
31. Breiman, L. Random Forests. *Mach. Learn.* **2001**, *45*, 5–32. [[CrossRef](#)]
32. Chen, T.; Guestrin, C. XGBoost: A Scalable Tree Boosting System. In Proceedings of the 22nd Acm Sigkdd International Conference on Knowledge Discovery and Data Mining, San Francisco, CA, USA, 13–17 August 2016; pp. 785–794. [[CrossRef](#)]
33. Hochreiter, S.; Schmidhuber, J. Long Short-Term Memory. *Neural Comput.* **1997**, *9*, 1735–1780. [[CrossRef](#)]
34. Sill, J.; Takacs, G.; Mackey, L.; Lin, D. Feature-Weighted Linear Stacking. *arXiv* **2009**, arXiv:0911.0460.
35. Homepage—U.S. Energy Information Administration (EIA). Available online: <https://www.eia.gov/> (accessed on 20 June 2022).
36. New York Independent System Operator (NYISO). Available online: <https://www3.dps.ny.gov/W/PSCWeb.nsf/All/298372E2CE4764E885257687006F39DF> (accessed on 20 June 2022).
37. BARON. Available online: https://www.gams.com/latest/docs/S_BARON.html (accessed on 20 June 2022).

Disclaimer/Publisher’s Note: The statements, opinions and data contained in all publications are solely those of the individual author(s) and contributor(s) and not of MDPI and/or the editor(s). MDPI and/or the editor(s) disclaim responsibility for any injury to people or property resulting from any ideas, methods, instructions or products referred to in the content.